# Measurement of the 3D particle velocity and temperature distribution induced by surface acoustic waves using V3V-Flex volumetric PIV and PLIF

J. König[1,*], C. Kykal[2], F. Kiebert[1], A. Boomsma[3], H. Schmidt[1]
1: IFW Dresden, SAWLab Saxony, P.O. 270116, 01171 Dresden, Germany
2: TSI GmbH, Neuköllner Str. 4, 52058 Aachen, Germany
3: Fluid Mechanics Research Instruments, TSI Incorporated, Shoreview, MN, USA

* Correspondent author: j.koenig@ifw-dresden.de

**Keywords**: DDPIV, acoustic streaming, acoustic radiation force, thermal-acoustic effects

ABSTRACT

Surface acoustic waves (SAWs) allow for tailored fluid and particle manipulation based on the acoustic streaming and the acoustic radiation force. A common application of SAWs is its utilization in microfluidics since high-frequency ultrasonic waves (up to 5 GHz) provide a very efficient means to induce fluid motion and a significant force on tiny particles within these scales. However, detailed knowledge about the influence of those high-frequency waves is still missing from the literature, regarding not only the acoustic streaming and scattering effects, but also the temperature effects induced in the fluid. For the first time, volumetric velocimetry and temperature measurements of the fluid flow induced by surface acoustic waves are presented, using a novel combination of a V3V-Flex system from TSI Inc. and planar laser induced fluorescence (PLIF). Using tomographic aperture encoded particle tracking velocimetry (TAPTV), the V3V-Flex system allows for measuring the 3D particle position with very low uncertainty (4.3 µm in *xy*-plane, 36 µm in depth) in a comparably large measurement volume of about (70 x 56 x 22) mm³. In this way, the acoustically-induced particle velocity was measured with high spatial resolution (0.06 mm³) in a simplified experimental setup consisting of a large glass cuvette filled with de-ionized water and a SAW-device at a frequency of 42.9 MHz. It is shown that the acoustic radiation force can be neglected for particles up to 21 µm in diameter, for this experimental configuration. The three-dimensional fluid flow induced via acoustic streaming is characterized by two velocity jets that penetrate deeply into the water with a velocity in the range of a few mm/s. Even though a very low electrical power level ($P_{el} \approx 7$ mW) is applied, a local temperature increase of the water, up to 0.85 K, within the measurement volume was determined. Our measurements have shown that the temperature increase locally coincides with the velocity jets, which experimentally confirms that acoustic energy absorption and acoustic streaming occur at the same time.

## 1. Introduction

In recent years, acoustic pressure waves induced by surface acoustic waves (SAWs) have attracted researchers' attention in order to separate micro particles or to mix small amounts of liquids, either by exploiting the acoustic radiation force or the acoustic streaming [3]. The main use of SAWs in fluid mechanics, biomedical or chemical analysis is usually considered to be in microfluidics, since SAW-devices with high frequencies (up to 5 GHz) can be easily integrated into lab-on-a-chip systems and provide a very efficient means to induce fluid motion or a

significant force acting on particles or living cells within these small scales [3]. Moreover, the SAW technology promises a complete microfluidic solution including sample preparation and analyte detection, offering remarkable prospects to biomedical applications [14,15].

Surface acoustic waves are mechanical waves with amplitudes of typically only a few nanometers, which propagate along on the surface of a piezoelectric substrate, e.g. lithium niobate ($LiNbO_3$). They are generated via the inverse piezoelectric effect by applying an electric field with high frequency to thin-film interdigitated transducers (IDT) deposited onto the surface. Once in contact with a liquid, the energy of the SAW radiates into the liquid, causing a bulk acoustic wave (BAW) that, in turn, drives a laminar fluid flow or deflects suspended particles in direction of the acoustic beam propagation due to the acoustic streaming [5] or the influence of the acoustic radiation force [2,8,9], respectively. The influence of both types of forces, depending on the physical properties of the particles and the fluids, has been usually studied at the microscale, e.g. see [2,3,8,9]. However, the size of the microfluidic devices is small compared to the attenuation length of the BAW and the SAW, which can cause acoustic reflections at the channel walls that strongly influence the resulting particle motion [4]. Hence, side effects are expected due to the acoustic reflections, making it difficult to apply any findings to another setup or to assess the acoustic streaming and the acoustic radiation force in detail.

Besides the influence of the physical properties of the particles and the fluid, another very important experimental condition remains to be dealt with in acousto-fluidics using ultrasonic waves; the temperature. Since most of the acoustic energy is absorbed into heat, either by the fluid or due to electromechanical losses in the piezoelectric substrate, a strongly localized temperature increase can occur that locally influence the physical properties of the fluid and, in turn, affects the propagation of the BAW through the fluid and the resultant velocity jet. With biomedical application in mind, a strongly localized temperature increase inside a microfluidic device might also harm biological samples, making the use of SAWs unsuitable for micro total analysis systems.

For the first time, particle velocity measurements and temperature measurements will be presented on a simplified experimental setup, in order to experimentally reveal thermo-fluidic effects, the resultant acoustic streaming and the actual influence of the acoustic radiation force originating from SAWs. For that reason, we took a novel approach that utilized a V3V-Flex system based on tomographic aperture encoded particle tracking velocimetry (TAPTV) for the 3-component volumetric measurement of the particle velocities, while the temperature distribution inside the fluid is mapped by using planar laser induced fluorescence (PLIF).

## 2. Experimental setup

In figure 1, a photo of the SAW-device used for the experiments is depicted. It is made of 128° YX lithium niobate ($LiNbO_3$) fixed on a printed circuit board (PCB) for electrical connection. On its surface thin-film (300 nm thickness) interdigitated electrodes of aluminum are deposited, the so-called interdigital transducer (IDT). The width of the electrodes as well as their distance to each other amount to a quarter of the wavelength $\lambda_{saw}$ of the SAW, which is determined by the geometrical periodicity of the IDT. For the present experiments the wavelength of the SAW is $\lambda_{saw} = 90$ µm. By applying an electric field with high frequency, $f = c_{saw}/\lambda_{saw}$, corresponding to the velocity $c_{saw}$ and the wavelength $\lambda_{saw}$ of the SAW, the inverse piezoelectric effect generates elastic deformations of the substrate's surface, so that SAWs are excited and propagate along the crystallographic *X*-axis of the chip to both sides of the IDT.

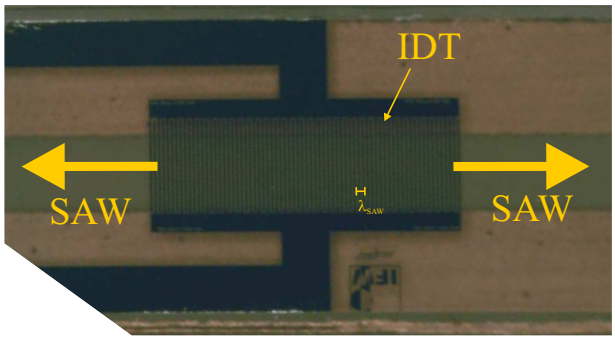


**Fig. 1** Photo of the SAW-device.

The simplified experimental setup is schematically depicted in figure 2. It consists of a large cuvette with inner dimensions (H x W x D) = (97 x 143 x 50) mm³. The piezoelectric substrate is immersed in the fluid at the right hand-side of the glass cuvette. The propagation of the SAWs to both sides of the IDT leads to two BAWs inside the fluid. The propagation angle of the BAWs is determined by the Rayleigh angle $\Theta_R$ that is given by the phase velocity $c_{saw}$ of the SAW and the speed of sound $c_{fluid}$ of the fluid. With the expected radiation characteristic of relatively small divergence of the BAWs, the two velocity jets induced by the BAWs propagate mainly along the *xy*-plane of the setup. The penetration depth of the BAWs and the velocity jets depends on the attenuation of the BAWs. Taking the shear and the bulk viscosity of water at 20°C into account, the attenuation length $\alpha$ of the BAWs amounts to approximately 21 mm at a frequency of 42.9 MHz. Therefore, the acoustically-induced velocity jets can be supposed to be unaffected by the limited size of the glass cuvette.

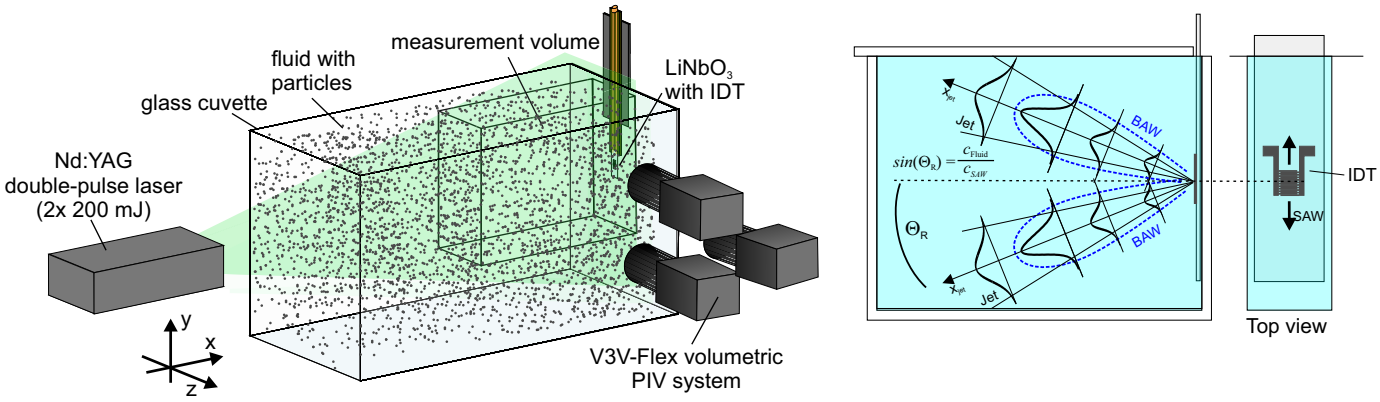


**Fig. 2**. (left) setup used for volumetric particle velocimetry and (right) sketch of the expected BAW and acoustically-induced velocity jets inside the glass cuvette when $LiNbO_3$ with the IDT is immersed in the fluid

In order to measure temperature and 3D velocity distributions inside the glass cuvette, planar laser induced fluorescence (PLIF) and a V3V-Flex system based on the tomographic aperture encoded particle tracking velocimetry (TAPTV) approach was combined. The V3V-Flex system is fundamentally based on the digital defocus particle image velocimetry (DDPIV) [6,12]. However, in contrast to the DDPIV using a pinhole mask [12] or the previous V3V-system with three cameras fixed in a triangular mount [11,13], no previous information about the imaging optics (distances, angle between the apertures) is required to reliably identify the particle position in the 3D. Hence, the TAPTV approach makes volumetric 3-component particle tracking available for varying measurement volume sizes and measurement resolution. As sketched in figure 2, an Nd:YAG dual cavity laser (Evergreen 200mJ, Quantel) was used to illuminate the fluid from the side, using a volume illumination and a thin laser light sheet for velocity and temperature measurements, respectively. To detect both, the light scattered from the suspended particles and the fluorescence light of the Rhodamine B dissolved in the fluid (concentration: 30 µg/L), either one or three cameras (8MP, pixel size 5.5 µm, TSI 630092) were used. For the PLIF-measurements, the camera lens (Nikon, 85mm f2.0) was equipped with an optical filter (550 nm long pass filter, TSI 610072) to suppress the excitation laser light. Camera lenses with a focal length of 85 mm and a small f-number of f/16 (Nikon f1.4) were used to get sharp images of all particles inside the entire glass cuvette during velocity measurement.

## 3. Calibration, measurement and evaluation procedure

### V3V-Flex volumetric velocity measurements

In order to calibrate the V3V-Flex system, a calibration target with artificial particles (dot spacing 2 mm) was placed inside the glass cuvette at well-known depth positions with a distance of

$\Delta z$ = 1 mm in between. At each calibration plane a calibration mapping function M($X,Y,z$) is obtained. Here, capital letters indicate pixel-coordinates, whereas lower-case letters indicate physical coordinates. Figure 3 illustrates the result of the calibration and the calibration signature graph. The signature graph shows the aperture specific origin for each camera, which is given by the center of the calibration target. On the left, the nominal magnification of each camera and the mean dewarping error are depicted. The latter represents the least squares error fit for the mapping function.

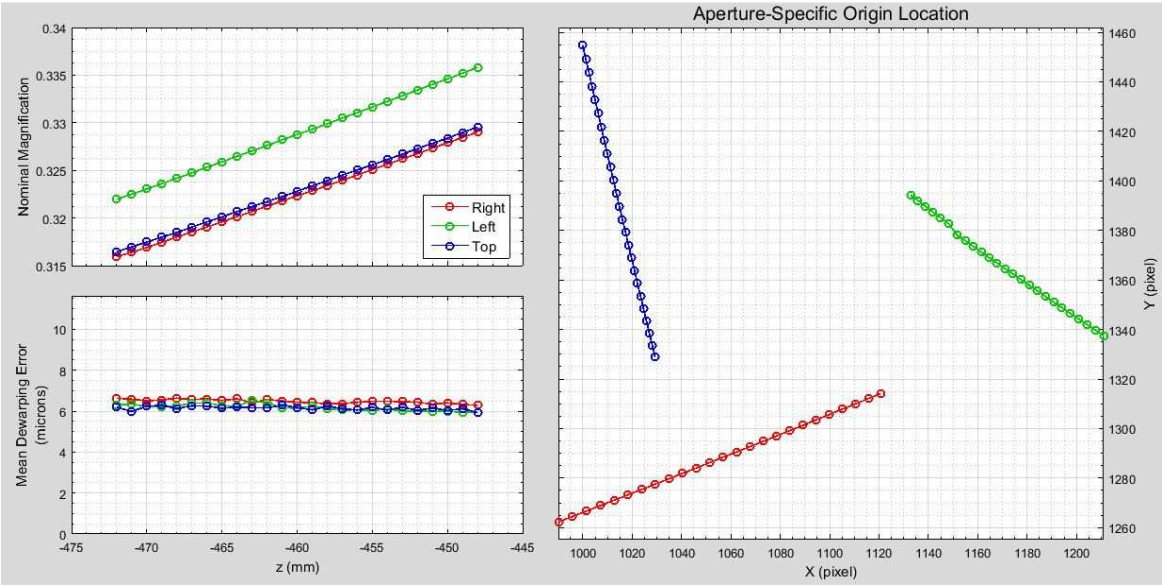


**Fig. 3:** Calibration result of the V3V-Flex system with 3 cameras.

During the flow measurements, up to 250x2 recordings were acquired at a maximum repetition rate of 15 Hz. The time interval $\Delta t$ between the double pulses of the laser was adjusted prior to the measurements in order to obtain particle images suitable for particle tracking at each individual parameter set, e.g. electrical power $P_{el}$ applied to the IDT. Either hollow glass spheres (mean diameter 10 µm, mean density 1.1 g/cm³) or silver-coated polystyrene particles (density 2.4 g/cm³) of different size were used as tracer particles. At each time of image capture ($t_0$, $t_0 + \Delta t$) the particle positions (X,Y) were identified in each image (6 images in total for each record) using a two-dimensional Gaussian interpolation for sub-pixel centroid accuracy. To determine the 3D particle positions, each particle image from the left aperture is mapped via the calibration $(x,y) = M(X,Y,z)$ into physical coordinates at three consecutive calibration planes. In a next step, a searching area in each other aperture is calculated based on the physical coordinates of the particle image from the left aperture back-projected to the other apertures using $M^{-1}(x,y,Z)$. Any particle images within this searching area, and from each aperture, are then mapped into physical space at the three corresponding calibration planes. Those particle images whom

intersect within a certain tolerance are considered as a particle match. If no particle match was found the particle image is evaluated by applying the same procedure to the next three consecutive calibration planes.

To determine the uncertainty of the 3D particle reconstruction positions, we performed an uncertainty analysis by propagating potential error sources via root sum squares. Uncertainty is due to a several experimental and algorithmic parameters including the number of cameras, the angle between cameras, the accuracy of the subpixel 2D Gaussian fit, magnification, particle size, pixel size, and least squares error of the calibration. Our uncertainty analysis yielded an uncertainty of 4.3 μm in the in-plane ($x,y$) directions, and 36 μm in the out-of-plane ($z$) direction.

After determining all particle positions in physical coordinates, the particles are tracked in 3D from the first image capture, at time $t_0$, to the second, at time $t_0 + \Delta t$, using a robust point matching [10]. For further evaluation, the randomly distributed particle velocity vectors were ensemble-averaged and interpolated onto a rectangular grid using Gaussian-weighted interpolation based on vector distance from the grid nodes. The minimum voxel size for the interpolation amounted to 2mm × 1mm × 1mm. By using an overlap between neighboring voxels of about 70% a minimum grid spacing of 0.3 mm was obtained. Hence, the acoustically-induced particle velocity could be analyzed with high spatial resolution of approximately 0.06 $mm^3$ inside the measurement volume, containing up to almost 1.6 million velocity vectors.

**PLIF- temperature measurements**

Calibration of the PLIF was conducted by heating up the fluids. Within a temperature range of approximately 20°C to 50°C at maximum, fluorescence intensity images were captured at five distinct temperatures. The expected linear relation between fluorescent light intensity and temperature could be found. For all measurements, the dye concentration (Rhodamine B) of about 30 μg/L was kept constant. During the temperature measurements, only one laser cavity was used at relatively low power to avoid any local temperature rise by laser light absorption. One hundred images were captured for each parameter set (electrical power level $P_{el}$) and averaged to reduce side effects of a temporal laser light intensity variation. The Insight 4G software from TSI Inc. was used to evaluate the PLIF images. Neither an absorption nor a laser pulse energy correction was applied. In order to reduce the influence of laser light absorption or a non-uniform laser light illumination, the local temperature increase was finally determined by subtracting the fluorescence intensity images captured when no SAW was excited, from the fluorescence intensity images captured during a certain electrical power level was applied to the IDT ($\Delta T = T_{OFF} - T_{ON}$).

## 4. Measurement results

*Flow and temperature behavior*

We first describe the 3D flow structure and temperature distribution. For this, a 3D velocity measurement result obtained in the large cuvette is depicted in figure 4(a). Hollow glass spheres suspended in de-ionized water were used as tracer particles and an electrical power level of $P_{el} \approx 7$ mW was applied to the IDT. Starting from the IDT position, two velocity jets propagate through the fluid, as already sketched in figure 2. The semi-angle between both jets amounts to approximately 22°, corresponding to the expected Rayleigh-angle. The green iso-surfaces represent areas with a velocity magnitude of 2.5 mm/s. Hence, the two velocity jets propagate deeply into the water with a relatively high velocity considering the very low electrical power level applied to the IDT. Moreover, a local temperature increase can be recognized at the central *z*-position as depicted in the temperature field illustrated in figure 4(b). The temperature increase locally coincides with the two velocity jets, which proves true that acoustic energy absorption and acoustic streaming occur at the same time. The origins of the temperature jets are obviously located at both ends of the IDT, at which the number of superimposed partial SAWs is at maximum, causing high acoustic energy at these local positions. Finally, even though a very low electrical power level of about $P_{el} \approx 7$ mW is applied, the local temperature increase amounts to 0.85 K inside the free propagating velocity jets.

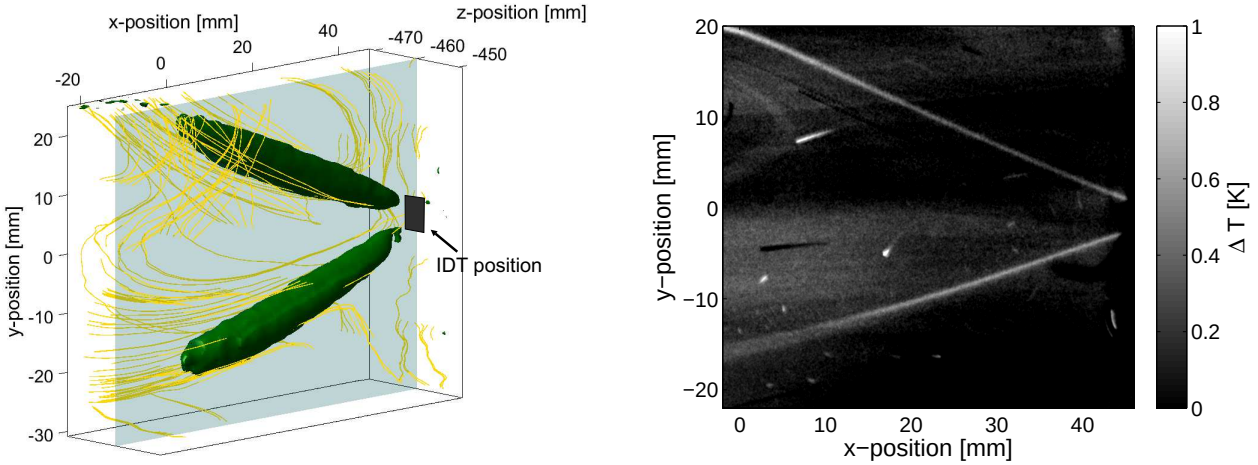


(a) (b)

Fig. 4 (a) measured volumetric velocity field and (b) temperature field at the center *z* position induced by a SAW when an electrical power level of about 7 mW is applied.; $\Delta T = T_{OFF} - T_{ON}$

*Acoustic radiation vs. acoustic streaming*

As mentioned above, SAWs are used not only to induce fluid flow via the acoustic streaming, but also to deflect particles suspended in the fluid by exploiting the acoustic radiation force. The influence of both forces depends on several experimental conditions, e.g. density and compressibility of the fluid and the particles. Another very important parameter is the ratio between size of the particles and wavelength of the bulk acoustic wave. In [9] the dimensionless number $\kappa = k \cdot d_P/2$, depending on the wavenumber $k$ of the BAW and particle diameter $d_P$, is used to illustrate the influence of the acoustic radiation force acting on polystyrene particles suspended in deionized water [9]. Based on the measurement results, a critical value $\kappa_{crit} = 1.2$ was found at which particles start to be deflected inside a microchannel due to the influence of acoustic radiation force. Below this critical value acoustic streaming dominates. Destgeer et al. confirmed that result and found $\kappa = 1.4$ at which particles experienced maximum acoustic radiation force [2]. Again, the influence of the acoustic radiation force vanishes for particle sizes yielding $\kappa < 1$ [2]. Considering the frequency of the acoustic wave used in the present experiments, a particle suspended in water should have a diameter of less than 10.7 µm ($\kappa = 1$). However, very small particles may produce particle images of poor quality, since very small numerical apertures (here: f/16) are necessary to get a sufficiently large measurement volume in depth for DDPIV. Therefore, measurements utilizing various particle sizes were conducted, not only to determine the influence of the acoustic radiation force, but also to find the largest diameter of the particles that still faithfully follow the fluid flow induced by the acoustic streaming.

According to [1], the acoustic radiation force for a travelling acoustic wave acts on particles, proportional to $\propto d_P^2$, if density of the fluid and the particles do not match. It applies: the higher the mismatch of the densities the higher the acoustic radiation force. For that reason, silver-coated polystyrene particles were applied in our experiments, whose density, 2.4 g/cm$^3$, significantly differ from that of water and produce particle images of sufficient quality even at small size. To distinguish between $\kappa < 1$, $\kappa \approx 1$ and $\kappa > 1$, three different particles of 3.5 µm, 11 µm and 21 µm in diameter were used for velocity measurements under same experimental conditions (fluid: de-ionized water, $P_{el} \approx 70$ mW). Thus, the resultant particle velocity might alter depending on $\kappa$. However, while higher velocities with increasing particle diameter might be expected, the axial jet velocity profiles, depicted in figure 5, show no obvious dependence on the particle diameter. Regardless of the particle diameter used for the velocity measurements, not only the maximum jet velocity remains nearly constant, but also the jet velocity profile.

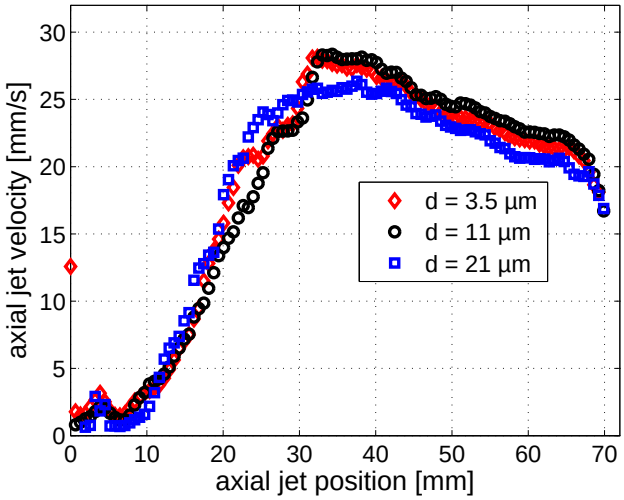


**Fig. 5** Axial jet velocity profile of the lower jet for three different sizes of silver-coated polystyrene particles

## 5. Summary

In this contribution, the application of a novel approach utilizing a V3V-Flex system and planar laser induced fluorescence (PLIF) for investigating the fluid flow and temperature distribution induced by SAWs in a large glass cuvette is reported. Though, only three of four cameras were used for the velocity measurements, the 3D position of individual particles is determined with very low uncertainty. The uncertainty of the particle position amounts to approximately 3.6 µm in the in-plane directions and 36 µm in the out-of-plane direction. Hence, the volumetric particle velocity induced by SAWs could be analyzed with a high spatial resolution down to 0.06 mm³, despite a comparably large measurement volume of about (70 x 56 x 22) mm³. The expected fluid flow, consisting of two narrow jets that propagate through the fluid, were determined. Both jets deeply penetrate into the water with velocities in the range of a few mm/s, even at a very low electrical power level of about 7 mW.

Based on PLIF measurements, a temperature increase was found that locally coincides with the velocity jets, showing that acoustic energy absorption and acoustic streaming occur at the same time. For an electrical power level of $P_{el} \approx 7$ mW, the local temperature increases up to 0.85 K within the measurement volume. In addition, to estimate the influence of the acoustic radiation force, velocity measurements were conducted using tracer particles of significantly different size. It was found that the axial velocity jet profile remains nearly constant even though the particle size exceeds a critical value. Obviously, the acoustic radiation force induced by a travelling bulk acoustic wave of 42.9 MHz frequency has minor influence on the resultant velocity of silver-coated particles suspended in de-ionized water up to 21 µm of particle diameter.

**Acknowledgment**

Funding by the German Federal Ministry of Education and Research under BMBF grant InnoProfile-Transfer 03IPT610A and by the Leibniz Association within the Joint Initiative for Research and Innovation (SAW-2014-IFW-1) is gratefully acknowledged.

## References

1. Annamalai S., Balachandar S, Parmar, MK (2014) Mean force on a finite-sized spherical particle due to an acoustic field in a viscous compressible medium. Phys. Rev. E 89: 053008
2. Destgeer G, Lee KH, Jung JH, Alazzamb A, Jin Sung H, (2013) Continuous separation of particles in a PDMS microfluidic channel via travelling surface acoustic waves (TSAW). Lab Chip 13: 4200
3. Ding, X et al (2013) Surface acoustic wave microfluidics. Lab Chip 13:3626-3649
4. Kiebert F, Schmidt H (2016) Particle Gradient Generation in a Microchannel Using a Single IDT, In Proceedings of the 18th International Conference on Ultrasonics, March 2016, Miami, USA
5. Lighthill J (1978) Acoustic streaming. J. Sound Vib. 61: 391-418
6. Pereira F, Gharib M, Dabiri D, Modarress D (2000) Defocusing digital particle image velocimetry: a 3-component 3-dimensional DPIV measurement technique. Application to bubbly flows. Exp. In Fluids (Suppl.1) 29: 84-87
7. Settnes M, Bruus H (2012) Forces acting on a small particle in an acoustical field in a viscous fluid. Physical Review E, 85(1):016327
8. Shi, J. et al. (2011) Three-dimensional continuous particle focusing in a microfluidic channel via standing surface acoustic waves (SSAW). Lab Chip 11: 2319-2324
9. Skowronek V, Rambach RW, Schmid L, Haase K, Franke T (2013) Particle deflection in a poly(dimethylsiloxane) microchannel using a propagating surface acoustic wave: size and frequency dependence. Analytical Chemistry, 85(20):9955–9959
10. Stellmacher M, Obermayer K (2000) A new particle tracking algorithm based on deterministic annealing and alternative distance measures. Exp. in Fluids 28: 506-507
11. Troolin D, Longmire E (2009) Volumetric Velocity Measurements of Vortex Rings from Inclined Exits. Exp. in Fluids 48(3): 409-420
12. Willert CE, Gharib M (1992) Three-dimensional particle imaging with a single camera Exp.in Fluids,12(6):353-58
13. Wolf E, Kähler CJ, Troolin DR, Kykal C, Lai W (2010) Time-resolved volumetric particle tracking velocimetry of large-scale vortex structures from the reattachment region of a laminar separation bubble to the wake. Exp. in Fluids, 50(4): 977–988
14. Yeo, LY, Chang, H-C, Chan PPY, Friend JR, (2011) Microfluidic Devices for Bioapplications. Small 7:12-48
15. Yeo, LY, Friend, JR (2014) Surface Acoustic Wave Microfluidics. Annu. Rev. Fluid Mech. 46:379-406